RESEARCH ARTICLE | SEPTEMBER 05 2024

Oligoyne bridges enable strong through-bond coupling and efficient triplet transfer from CdSe QD trap excitons for photon upconversion *⊗*

Tsumugi Miyashita ⁽¹⁾; Sheng He ⁽¹⁾; Paulina Jaimes ⁽¹⁾; Alexey L. Kaledin ⁽¹⁾; Maria Fumanal ⁽¹⁾; Tianquan Lian ⁽¹⁾; Ming Lee Tang ⁽¹⁾



J. Chem. Phys. 161, 094707 (2024)

https://doi.org/10.1063/5.0223478

A CHORUS





Articles You May Be Interested In

On the size-dependence of CdSe nanocrystals for photon upconversion with anthracene

J. Chem. Phys. (September 2020)

Upconverting core-shell nanocrystals with high quantum yield under low irradiance: On the role of isotropic and thick shells

J. Appl. Phys. (November 2015)

Electronic properties of linear carbon chains: Resolving the controversy

J. Chem. Phys. (March 2014)





Oligoyne bridges enable strong through-bond coupling and efficient triplet transfer from CdSe QD trap excitons for photon upconversion

Cite as: J. Chem. Phys. 161, 094707 (2024); doi: 10.1063/5.0223478 Submitted: 14 June 2024 · Accepted: 12 August 2024 ·







Published Online: 5 September 2024

Tsumugi Miyashita, D Sheng He, D Paulina Jaimes, D Alexey L. Kaledin, A D Maria Fumanal, D



Tianguan Lian, 2,a) D and Ming Lee Tang 1,3,a)

AFFILIATIONS

- Department of Biomedical Engineering, University of Utah, Salt Lake City, Utah 84112, USA
- ²Department of Chemistry, Emory University, Atlanta, Georgia 30322, USA
- Department of Chemistry, University of Utah, Salt Lake City, Utah 84112, USA
- ⁴The Cherry L. Emerson Center for Scientific Computation, Emory University, 1515 Dickey Drive Northeast, Atlanta, Georgia 30322, USA
- ⁵Departament de Ciència de Materials i Química Física and IQTCUB, Facultat de Química, Universitat de Barcelona, Martí i Franquès 1, E-08028 Barcelona, Spain
- a) Authors to whom correspondence should be addressed: tlian@emory.edu and minglee.tang@utah.edu

ABSTRACT

Polyyne bridges have attracted extensive interest as molecular wires due to their shallow distance dependence during charge transfer. Here, we investigate whether triplet energy transfer from cadmium selenide (CdSe) quantum dots (QDs) to anthracene acceptors benefits from the high conductance associated with polyyne bridges, especially from the potential cumulene character in their excited states. Introducing π -electron rich oligoyne bridges between the surface-bound anthracene-based transmitter ligands, we explore the triplet energy transfer rate between the CdSe QDs and anthracene core. Our femtosecond transient absorption results reveal that a rate constant damping coefficient of β is 0.118 ± 0.011 Å⁻¹, attributed to a through-bond coupling mechanism facilitated by conjugation among the anthracene core, the oligoyne bridges, and the COO^{\ominus} anchoring group. In addition, oligoyne bridges lower the T_1 energy level of the anthracene-based transmitters, enabling efficient triplet energy transfer from trapped excitons in CdSe QDs. Density-functional theory calculations suggest a slight cumulene character in these oligoyne bridges during triplet energy transfer, with diminished bond length alternation. This work demonstrates the potential of oligoyne bridges in mediating long-distance energy transfer.

Published under an exclusive license by AIP Publishing. https://doi.org/10.1063/5.0223478

INTRODUCTION

Conjugated molecular wires with high conductance are interesting model systems that establish the limits of charge and energy transfer in soft matter. Molecular wires also play an important role in hybrid organic-inorganic molecular-nanocrystal systems where energy or charge must be transferred efficiently. Examples of large tunneling transmission values are found in all-carbon sp-hybridized linear chains in the form of polyynes or cumulenes. Polyynes are a series of alternating single and triple carbon bonds, while cumulenes are a chain of connected carbon-carbon double bonds with dimin-

ished bond alternation. Compared to saturated alkane bridges and phenylene-based molecular wires, the exponential attenuation factor, β , for the distance-dependent charge transfer rates for polyynes is $0.17-0.23 \text{ Å}^{-1}$, lower than 0.94 Å^{-1} for methylene $(-CH_2-)_n^2$ and 0.42 Å^{-1} for p-phenylene.^{3,4}

Here, we investigate if the high conductance associated with polyynes for charge transfer applies to triplet energy transfer (TET) from CdSe nanocrystal donors to anthracene acceptors. This is a model system for photon upconversion, where incoherent sources of light, e.g., from the sun, can be combined via triplet-triplet annihilation (TTA) to produce high energy photons. Other than the low damping coefficient β in a polyvne bridge, we were interested in the possibility that excited state geometries might involve a cumulene-based resonance contributor. Cumulene character in the excited state of polyyne bridges offers the tantalizing possibility of enhanced triplet energy transfer with increasing carbon chain length. Typically, coherent tunneling processes decay exponentially with distance, but the reversed bond-length alternation in cumulenes results in the opposite trend, where single molecule conductance can increase with the length of the molecular wire. Scanning tunneling microscopy break junction (STM-BJ) methods have shown either increasing conductance with increasing length⁵ or length independent single-molecule conductance in cumulenes anchored by thioanisole to gold electrodes.⁶ Nonequilibrium Green's function density-functional theory methods predict either ballistic transport⁷ or an inverse relationship between charge transmission and length.8

In related work with organic donor–acceptor complexes, Zieleniewska reported an increase in the rates of charge recombination with increasing carbazole–oxadiazole distances bridged by polyynes $(n=1-4).^{10}$ This unusual distance dependence was explained by increased accessibility to low-lying bridge states with increasing bridge length/conjugation and calculations suggesting cumulenic character in the bridge in the excited state that induced strong vibronic coupling between the carbazole donor and oxadiazole acceptor. In a separate study, Milani *et al.* showed that polyynes terminated with conjugated π -systems showed cumulene character with the modification of bond length alternation (BLA). ¹¹

Long, linear polyynes must be stabilized with bulky end-caps, e.g., pyridyl (n = 4), $^{1,12-14}$ bulky pyridyl (n = 24), 15,16 and BF₂ formazanate dyes (n = 10).¹⁷ This means synthetic accessibility to long, symmetric polyynes is possible, whereas asymmetric polyynes are less tractable, limiting charge or energy transfer measurements to shorter polyynes. For example, the first reports on asymmetrically functionalized acetynyl and butadiynyl (n = 1 and 2) bridges in 1997^{18} were followed by n = 1-4 oligovne groups between the N,N-diisopropylanilino donor and the 1,1,4,4-tetracyanobuta-1, 3-diene (TCBD) acceptor from Štefko et al. 19 Vail et al. measured a β = 0.06 Å⁻¹ for the back electron transfer rates between a Zn-porphyrin donor and fullerene acceptor bridged by alkyne groups, where n = 2, 3, and 4. This low distance dependence was attributed to the strong electronic coupling between the C₆₀ acceptor, the oligonol bridge, and the phenyl group of the porphyrin.²

Here, rigid acetylene bridges are explored for enhancing triplet energy transfer (TET) between the nanocrystal donor and transmitter acceptor ligands for photon upconversion. Three anthracene-based transmitter ligands with n=0,1, and 2 are employed: 9-anthracene carboxylic acid (9ACA), 9-carboxylic acid acetylene anthracene (CAA), and 9-carboxylic acid di-acetylene anthracene (CDAA), respectively. Our steady-state photon upconversion measurements show that the upconversion quantum yield (QY) with 532 nm excitation using CdSe QD donors with 2,5,8,11-tetra-tert-butylperylene (tBu_4P) emitters decreases from 9.88% to 3.08% to 1.07% as n increases from 0 to 2 with 9ACA, CAA, and CDAA transmitter ligands, respectively. Note that 50% is the maximum upconversion QY. In addition, femtosecond transient absorption (TA) measurements show that the rate of TET from QD to the transmitter, TET₁ (k_{TET1}), shows a shallow distance dependence. The

damping coefficient β for TET₁ is 0.118 \pm 0.011 Å⁻¹, which is 4–6 times lower than that using the phenyl spacer with an anthracene transmitter. Li and co-workers in 2016 demonstrated that when the distance between CdSe QDs and the anthracene transmitter ligand is increased by adding the rigid phenyl bridges, the TET₁ rate constant is distance dependent following the Dexter energy transfer model with the damping coefficient, $\beta = 0.43 \pm 0.07 \text{ Å}^{-1.21}$ Another study shows that when phenylene bridges are added between the CdSe QD donor and anthracene acceptor, the triplet energy transfer pathway changes from tunneling to a hopping mechanism over the 1 nm Dexter distance.²² They also calculated that the damping coefficient β is 0.7236 \pm 0.0005 Å⁻¹ during the tunneling mechanism. Our calculations show the coupling between CdSe QDs and the anthracene core with polyyne spacers is dominated by the COO[⊕] anchoring group, enabled by the conjugation between the acetylene bridge and the anthracene core. In addition, there is slight cumulene character in CAA and CDAA during TET, where bond length alternation is diminished. This work demonstrates that the acetylene spacer can extend the delocalization of triplet excitons between photosensitized donors and acceptors.

Triplet-triplet annihilation (TTA) based photon upconversion can convert two lower energy input photons to a higher energy photon. TTA can be used to enhance the performance of organic light emitting diodes (OLEDs), 23,24 photovoltaics, $^{25-27}$ and biomedical applications. 28,29 Hybrid molecule–nanocrystal systems for TTA based photon upconversion take advantage of the small singlet–triplet energy splitting of excitons in semiconductor nanocrystals, or quantum dots (QDs). $^{30-32}$ There are multiple steps in the TTA based photon upconversion, including the first triplet energy transfer from the photosensitizer QDs to the transmitter ligand molecule (TET1), the second triplet energy transfer from the transmitter ligand to the emitter molecules (TET2), and the triplet–triplet annihilation (TTA) between the emitter molecules. The total photon upconversion quantum yield, $\Phi_{\rm UC}$, can be defined as written in the following equation:

$$\Phi_{\text{UC}} = \eta \times \Phi_{\text{TETI}} \times \Phi_{\text{TET2}} \times \Phi_{\text{TTA}} \times \Phi_{\text{FL}}, \tag{1}$$

where η is the spin statistical factor defining the probability of forming a bright singlet state from a pair of annihilating triplet states. Φ_{TET1} is the triplet energy transfer efficiency from the photosensitizer to the transmitter ligand. Φ_{TET2} is the triplet energy transfer efficiency from the transmitter ligand to the emitter. Φ_{TTA} is the efficiency of the triplet–triplet annihilation and Φ_{FL} is the fluorescence efficiency of the emitters.

Figure 1(a) illustrates the TTA based photon upconversion process in this work. In the energy diagram, 2.68 nm diameter CdSe QD with the first exciton ($1S_{3/2}$) transition at 529 nm is photoexcited with 532 nm/2.34 eV photons at the band edge (see transmission electron microscopy image and the size distribution in Fig. S1). Note that 9ACA, CAA, CDAA (n = 0, 1, and 2 acetylene groups, respectively), DPA, and tBu_4P do not absorb this green excitation. Our previous work has shown that both bright and dark excitons at the band edge in CdSe QDs have triplet character.³³ The triplet exciton is transferred to the transmitter ligands (9ACA, CAA, or CDAA) and then to the DPA or tBu_4P emitters via TET₁ and TET₂, respectively. Two emitter molecules in their triplet excited state can undergo TTA to create a singlet, emitting a 3.06 or 2.47 eV

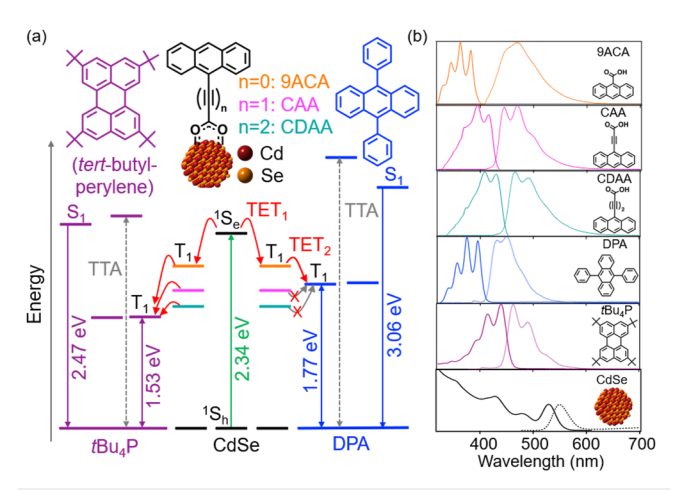


FIG. 1. (a) The energy diagram shows the first triplet energy transfer (TET $_1$) step from the CdSe sensitizer excited with 2.34 eV to the transmitter ligands (9ACA, CAA, or CDAA), which have different T $_1$ energy levels (orange for 9ACA, magenta for CAA, and cyan for CDAA). Then, the second triplet energy transfer (TET $_2$) from the transmitter ligands to the emitters (DPA or tBu_4P) involved in photon upconversion via triplet–triplet annihilation (TTA). 3.06 eV (blue line) or 2.47 eV (purple line) photon upconversion luminescence are observed depending on the emitter molecules DPA or tBu_4P , respectively. (b) Normalized absorption (solid), fluorescence (dashed), excited with 375 nm. 9ACA (orange), CAA (magenta), CDAA (cyan), DPA (blue), and tBu_4P (purple) are prepared in deoxygenated tetrahydrofuran solution, and CdSe is prepared in deoxygenated toluene solution. All samples are prepared at room temperature (RT) in the nitrogen glovebox with the molecular absorption peaks or QD first exciton (1S $_{3/2}$) wavelength at 529 nm < 0.1 to eliminate the inner filter effect.

photon from DPA or tBu_4P , respectively. Figure 1(b) shows the steady-state absorption and fluorescence with 375 nm excitation of the transmitter ligand molecules in tetrahydrofuran and CdSe in toluene. The novel CAA and CDAA transmitter ligands and nanocrystals are synthesized in house (see the details in Sec. 2 of the

supplementary material). The red shift in the absorption and fluorescence maxima observed as n increases from 0 to 2 in the transmitter ligand molecules is due to the extended π -conjugation (Table I). Compared to 9ACA, CAA and CDAA show more distinct vibrational peaks in fluorescence. This is because, at the S_0 and S_1 minima, the anthracene core in 9ACA has different dihedral angles with respect to the COOH group at the 9-position.³⁴ We found that this dihedral angle goes from 58° in S_0 to 29° torsion in S_1 (Fig. S2). In contrast, in CAA and CDAA, both S₀ and S₁ minima have COOH coplanar with respect to the anthracene core; therefore, the S₁ minima does not shift with respect to the S₀ (Fig. S2). This results in a smaller Stokes shift and more distinct peaks in the fluorescence spectrum (Fig. S3). According to the ωb97xd/6-31g(d) calculations, phosphorescence peaks also bathochromically shift as more acetylene groups are added, from 807, 884, to 915 nm (Table I). The fluorescence quantum yield, Φ_{FL} , for 9ACA, CAA, and CDAA is 42.8%, 60.1%, and 40.0%, respectively. The CdSe nanocrystals show absorption peaks at 480 and 430 nm that may correspond to the $2S_{3/2}$ and $1S_{1/2}$ exciton transitions, respectively, as discussed below.³⁵ The emission at > 600 nm is attributed to trapped excitons with lower energy.

Steady-state photon upconversion was conducted with 532 nm CW lasers for 2.7 µM CdSe QDs functionalized with 9ACA, CAA, or CDAA in the presence of 3 mM DPA or *t*Bu₄P emitters in toluene. The average number of ligands per QD is calculated from the steadystate absorption spectrum after the ligand exchange (Fig. S4) by using the molecular extinction coefficient, which is obtained following previously reported work (see the details in Fig. S5).³⁸ As shown in Fig. S4, the average number of surface bound 9ACA, CAA, and CDAA ligands is 10, 24, and 17, respectively, for samples with the highest upconversion QY, correspond to the most efficient TET. The QD-transmitter CdSe-9ACA (n = 0) photosensitizer produces 3.06 and 2.47 eV photons via TTA with both DPA and tBu₄P emitters, respectively, under 532 nm excitation (Fig. 2 top panel), with comparable upconversion quantum yields (UCQYs) at 10.7% and 9.88%, respectively, calculated from Eq. S1 (Table I). Note that the maximum theoretical value of the UCQY is 50% due to the two-to-one

TABLE I. Important parameters for TTA-based photon upconversion with anthracene transmitter ligands of different numbers of acetylenes.

Transmitter ligand	$\lambda_{abs} (nm)^a$	$\lambda_{FL} (nm)^b$	$\lambda_{Phos} (nm)^{c}$	$T_1 (eV)^d$	Φ _{FL} (%) ^e	Φ_{UC} with DPA (%) ^f	$\Phi_{\rm UC}$ with $t{\rm Bu_4}$ P (%) ^g	Distance (Å) ^h	$k_{TET} (\mu s^{-1})^i$
9ACA	382	436	807	1.83	42.8	10.7	9.88	1.54	10.3 ± 0.53
CAA	416	444	884	1.63	60.1	0.02	3.08	4.28	8.72 ± 3.44
CDAA	430	465	915	1.56	40.0	0.00	1.07	7.02	5.34 ± 0.79

^aThe absorption peak wavelength of the lowest energy.

^bThe fluorescence peak wavelength of the highest energy.

^cThe vertical phosphorescence peak wavelength from the ωb97xd/6-31g(d) calculations method.

 $^{^{\}rm d}T1$ energy level by DFT calculations at $\omega b97xd/6\text{--}31g(d)$ level.

eRelative fluorescence quantum yield excited at 375 nm. DPA is used as a reference, with a fluorescence quantum yield of 90%.36

^fPhoton upconversion quantum yield with a 3 mM DPA/toluene emitter excited at 532 nm. The theoretical maximum value is 50%. The photoluminescence quantum yield of the DPA reference is 90% in toluene excited at 375 nm (Eq. S1).

gPhoton upconversion quantum yield with a 3 mM tBu4P/toluene emitter excited at 532 nm. The photoluminescence quantum yield of the tBu4P reference is 70% in toluene excited at 405 nm 37

^hThe distance is reported to be the acetylene spacer length between the anthracene core and the carboxylic acid ligands.

ⁱThe intrinsic rate constant of the triplet energy transfer from QDs to the transmitter ligands.

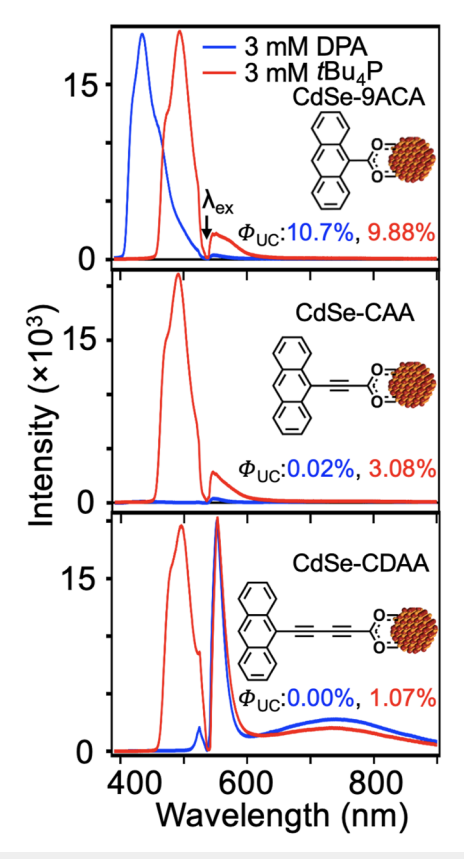


FIG. 2. Photon upconversion luminescence spectra of CdSe-9ACA, CdSe-CAA, and CdSe-CDAA with 3 mM DPA in toluene solution (blue) and with 3 mM tBu_4P in toluene solution (red). The photon upconversion quantum yield (Φ_{UC}) with 3 mM DPA emitter (blue) for CdSe-9ACA, CdSe-CAA, and CdSe-CDAA is 10.7%, 0.02%, and 0.00%, respectively. The Φ_{UC} with 3 mM tBu_4P emitter (red) for CdSe-9ACA, CdSe-CAA, and CdSe-CDAA is 9.88%, 3.08%, and 1.07%, respectively. The maximum theoretical value of Φ_{UC} is defined to be 50%. All samples are prepared in the nitrogen glovebox and excited at 532 nm.

photon process of TTA based photon upconversion. Compared to CdSe-9ACA, CdSe-CAA and CdSe-CDAA do not perform upconversion with the DPA emitter (blue curves in Fig. 2). Note that QD band edge emission at 550 nm and trap state emission at 750 nm are observed when using CdSe-CDAA (Fig. 2, bottom panel; the 532 nm is notched). This is due to higher QD concentration and the higher excitation power used for the upconversion measurement of CdSe-CDAA (Sec. 4.2 of the supplementary material). Upon changing the emitter from DPA to tBu₄P and, thus, lowering the T₁ energy level from 1.77 to 1.53 eV, a downhill energy cascade from CAA or CDAA to tBu₄P is expected, as TET₂ is no longer uphill such as in the case of DPA. As shown in the red curves in Fig. 2, both CdSe-CAA and CdSe-CDAA show 2.47 eV photon upconversion luminescence with 532 nm excitation in the presence of the perylene emitter, with UCQYs of 3.08% and 1.07% compared to negligible upconversion with DPA. We assume that this is because the T₁ energy level of CAA and CDAA is below 1.77 eV (T₁ of DPA) and above 1.53 eV $(T_1 \text{ of } tBu_4P)$, thus allowing TET₂ from CAA or CDAA to tBu_4P but not to DPA. Our calculations assign the decrease in T₁ energy level

from 1.83 eV in 9ACA to 1.63 eV in CAA and to 1.56 eV in CDAA, consistent with our photon upconversion results (Table I). It is interesting to compare the fact that there is no photon upconversion with the DPA emitter from the acetylene bridged transmitter ligands here, whereas the phenyl spacer samples show photon upconversion with DPA. This indicates that acetylene lowers the T₁ energy level of the anthracene core, while the phenyl group causes little perturbation. Table S1 compares the UCQY between acetylene and phenyl spacers. Taking into account the lower tBu_4P fluorescence quantum yield of 70% compared to DPA's 90% and also the fact that smaller CdSe QDs with a larger driving force for TET were used with the phenylene bridges, the acetylene spacer shows a higher UCQY for all samples with the tBu_4P emitter, in contrast to the phenyl-bridged samples with the DPA emitter.

The threshold intensity is another important factor for photon upconversion. The threshold excitation density is defined as the minimum incident power for the transition from a quadratic to a linear regime when plotting the upconverted emission against the excitation power density. In the quadratic regime, most of the triplets decay unimolecularly, while in the linear regime, TTA dominates. Figure S6 shows the upconverted 2.5 eV emission from 3 mM *t*Bu₄P sensitized by 2.7 μM CdSe-9ACA, CdSe-CAA, and CdSe-CDAA vs the power density using 532 nm excitation. The experimental threshold excitation density increases in the order of CdSe-9ACA, CdSe-CAA, and CdSe-CDAA, with values of 2800, 3700, and 6100 mW/cm², respectively. This trend is anticorrelated with UCQY with the *t*Bu₄P emitter for CdSe-9ACA, CdSe-CAA, and CdSe-CDAA, which is 9.88%, 3.08%, and 1.07%, respectively. All UCQY reported here is in the linear regime, where UCQY is the constant

To investigate the triplet energy transfer mechanism in the acetylene spacer samples, femtosecond (fs) transient absorption (TA) was conducted with CdSe, CdSe-9ACA, CdSe-CAA, and CdSe-CDAA in toluene. The samples are pumped at 530 nm, which selectively excites the CdSe first exciton but not 9ACA, CAA, or CDAA. Details of the experiment setup are provided in Sec. 5.1 of the supplementary material. Figure 3(a) shows the TA spectra of CdSe-CAA from 0.5 ps to 0.3 µs. TA spectra for other samples (CdSe, CdSe-9ACA, and CdSe-CDAA) are shown in Fig. S7I. At early delay times, <1 ns, the TA spectra for all samples are dominated by the ground state bleach (GSB) at 425, 480, and 530 nm and the excited state absorption (ESA) at 450 nm. Since only the 1S electron in the CdSe conduction band is excited under a 530 nm pump, the 425, 480, and 530 nm GSB can be assigned to the bleaching of the $1S_{1/2}$, $2S_{3/2}$, and 1S_{3/2} exciton transitions that involve the 1S electron, consistent with the CdSe ground state absorption in Fig. 1(b). The 450 nm ESA may be caused by the spectral red shift induced by the Stark effect in the excited state.³⁹ Compared to the pure CdSe sample, the presence of the transmitter ligands (9ACA, CAA, or CDAA) leads to faster recovery of the GSB signals and the appearance of new ESA signals at late delay time (>0.2 µs), as shown by the blue dashed spectrum in Fig. 3(a). To clearly observe the new ESA signals, nanosecond (ns) TA measurements with longer delay times were conducted, and the spectrum from 2 to 250 µs is shown in Fig. S8. Figure 3(b) shows the ESA spectra of 9ACA, CAA, and CDAA obtained from the smoothed ns-TA spectra of CdSe-9ACA, CdSe-CAA, and CdSe-CDAA averaged at 10–11 µs when there is no CdSe contribution as discussed below. These ESA spectra show clear peaks at 435, 450,

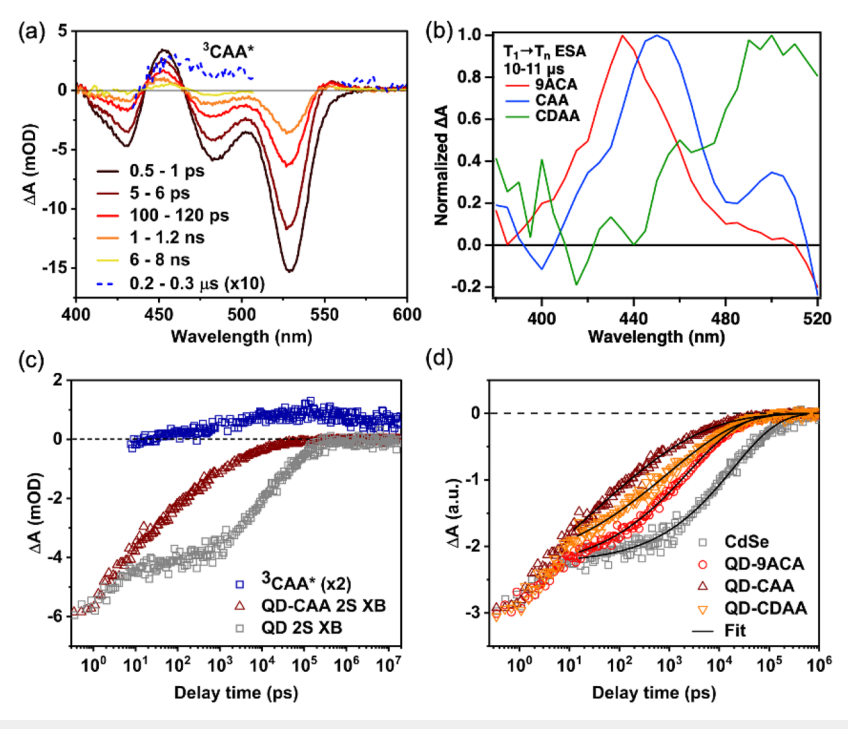


FIG. 3. (a) fs-TA spectra for CdSe-CAA in toluene excited at 530 nm. (b) T_1 to T_n ESA spectra for CdSe-9ACA (red), CdSe-CAA (blue), and CdSe-CDAA (green) obtained from ns-TA excited at 532 nm. (c) Transient kinetics of $2S_{3/2}$ exciton bleach (2S XB, brown up triangle) and CAA triplet (3 CAA * , dark blue square) in CdSe-CAA. Also shown is the 2S XB in the pure CdSe sample (gray square). (d) Scaled 2S XB kinetics in CdSe (gray square), CdSe-9ACA (red circle), CdSe-CAA (brown up triangle), and CdSe-CDAA (orange down triangle). The black curves are fitting to the kinetics. After considering the average number of ligands on the CdSe surface, the intrinsic triplet energy transfer rate constants from the fitting kinetics are obtained as $10.3 \pm 0.53 \, \mu s^{-1}$ for CdSe-9ACA, $8.72 \pm 3.44 \, \mu s^{-1}$ for CdSe-CAA, and $5.34 \pm 0.79 \, \mu s^{-1}$ for CdSe-CDAA.

and 490 nm for 9ACA, CAA, and CDAA, respectively. The CdSe-9ACA ESA spectrum matches well with the previous report on the 9ACA T₁ to T_n absorption spectrum, ^{38,40} which suggests that these late time ESA spectra in Figs. 3(b) and S8 are the triplet excited state absorption in 9ACA, CAA, and CDAA. Together, the faster GSB recovery in QD and the triplet formation in the transmitter ligands confirm the TET₁ step, as expected in Fig. 1(a). From the ns-TA data (Fig. S9), the lifetime of the triplet in 9ACA, CAA, and CDAA is found to be 288, 164, and 46 μs, respectively (details of the fitting are provided in Sec. 5.2 of the supplementary material). This shorter triplet lifetime as the number of acetylenes increases results in that the UCQY decreasing from 9ACA to CAA to CDAA since the TET₂ efficiency decreases. This is in line with reports that the non-radiative decay rates of polynes increase as *n* increases. ^{10,18,41–43}

To further investigate the influence of the acetylene spacer on TET_1 , we now focus on the TET_1 kinetics in the three samples. These triplet energy transfer kinetics can be followed by both the band edge exciton decay in the QD part and the triplet formation in the transmitters. The exciton kinetics are monitored at the $2S_{3/2}$ exciton bleach (2S XB) position at 480 nm to avoid the scattered pump light (details in Sec. 5.1 of the supplementary material), and the transmitter triplet kinetics are obtained by subtracting out the overlapped QD signal as detailed in Sec. 5.3 of the supplementary material. Note that although both band edge excitons and trapped excitons (electron in the conduction band and hole in trap states) can contribute

to the GSB signal in CdSe QDs and both can act as triplet donors,⁴⁰ it is unnecessary to separate their contributions in this study since the difference in TET₁ between the three samples is introduced only by the transmitters or by the acetylene spacers. Figure 3(c) shows the 2S XB kinetics in pure CdSe and CdSe-CAA. The initial decay part (<10 ps) is independent of the presence of acceptors and is the same in all the samples [Fig. 3(d)]. Thus, this early decay is likely due to biexciton Auger recombination ^{30,44} rather than acceptor-induced charge or energy transfer. However, CdSe-CAA shows much faster 2S XB decay than pure CdSe at > 10 ps. Meanwhile, the CAA triplet signal (³CAA²) shows growth kinetics that agree well with the QD 2S XB decay kinetics, which are more clearly shown in Fig. S13. Furthermore, the ³CAA* signal reaches its peak amplitude when the 2S XB signal decays to 0. The same phenomenon was observed for CdSe-9ACA, as shown in Secs. 5.5 and 5.6 of the supplementary material. For CdSe-CDAA, the ³CDAA^{*} kinetics were not available due to decreased signal intensity in the femtosecond TA experiment (Fig. S7Ih). Nevertheless, based on the results of CdSe-9ACA and CdSe-CAA, it is expected that the faster 2S XB decay reflects the TET₁ process in all three samples. Note that our previous studies have shown that the adsorption of transmitters on QD surfaces through the carboxylic group does not introduce other decay pathways such as electron trapping. 45-47 Figure 3(d) compares the 2S XB kinetics in CdSe-9ACA, CdSe-CAA, CdSe-CDAA, and pure CdSe

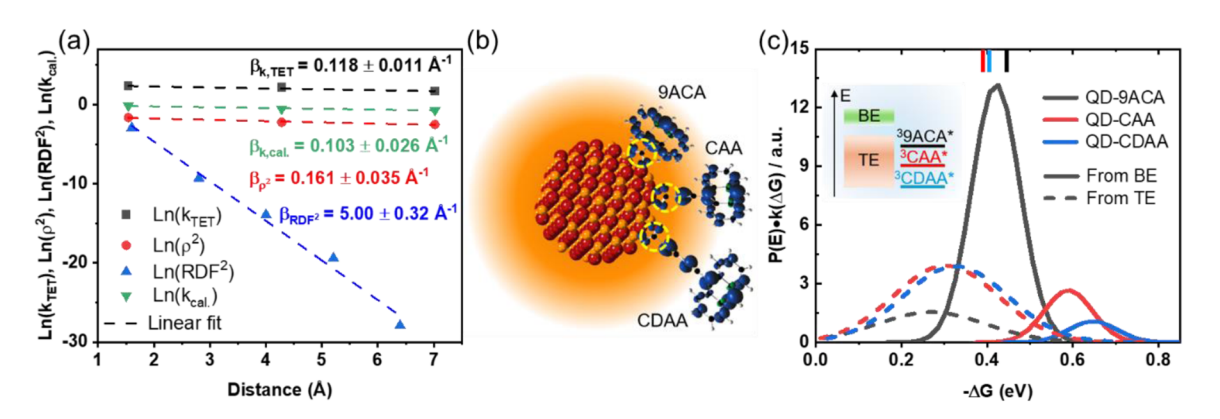


FIG. 4. (a) The Ln value of the intrinsic triplet energy transfer rate constant (k_{TET} , black squares), the squared spin density (ρ^2 , red dots), the squared QD exciton radial distribution function (RDF,² blue up triangles), and the calculated TET rate constant ($k_{Cal.}$, green down triangles), plotted as a function of the QD-transmitter distance. The dashed lines are linear fits to the Ln values. (b) Schematic of the triplet energy transfer coupling between CdSe QD and 9ACA, CAA, and CDAA. The orange shadow represents the RDF of the band edge exciton in CdSe. The spin density distribution of the T₁ state in 9ACA, CAA, and CDAA is shown. The yellow dashed circle indicates the integration volume of the spin density (ρ) around the anchoring COO[©] group in each transmitter. (c) Calculated TET rate constant as a function of driving force from band edge excitons (BE, solid lines) and trapped excitons (TE, dashed lines). The colored bars at the top x-axis indicate the reorganization energy λ in 9ACA (black), CAA (red), and CDAA (blue). Inset: schematic of energy level alignment in the QD-transmitter complexes. Green area: energetic distribution of band edge exciton and orange area: energetic distribution of trapped exciton.

QDs. The kinetics are clearly non-single exponential and can be well fitted by a stretched exponential decay function, as shown in the following equation:

$$A(t) = A_0 e^{-\left(\frac{t}{\tau_0}\right)^{\beta'}}. (2)$$

In Eq. (2), A_0 is the signal amplitude, τ_0 is the effective decay time constant, and β' describes the distribution of τ_0 , or its reciprocal, the decay rate constant k. Fitting details are given in Sec. 6 of the supplementary material. The fit results are shown in Fig. 3(d), and the parameters are listed in Table S2. The stretch exponential decay function reflects a broad distribution of TET₁ pathways, such as transfers from band edge excitons and trapped excitons with different energies. Overall, the fitting yields a phenomenological TET₁ efficiency of 80%–90% for all three samples (Table S2). Taking into account the average number of transmitter ligands adsorbed on each QD, we obtain the intrinsic triplet energy transfer rate constants (i.e., rate constant per acceptor): $10.3 \pm 0.53 \,\mu\text{s}^{-1}$ in CdSe-9ACA, $8.72 \pm 3.44 \,\mu\text{s}^{-1}$ in CdSe-CAA, and $5.34 \pm 0.79 \,\mu\text{s}^{-1}$ in CdSe-CDAA, as summarized in Table I. These rate constants are consistent with literature reports of the same process in CdSe QD and 9ACA. $^{30.48,49}$

Previous studies have suggested that triplet energy transfer between CdSe QDs and 9ACA follows the Dexter energy transfer mechanism, $^{30,40,49}_{}$ where the rate constant k_{TET} can be described by $^{50-52}$

$$k_{TET} = \frac{2\pi}{\hbar} |V|^2 FCWD. \tag{3}$$

In Eq. (3), FCWD is the Frank–Condon overlap weighted density of states. V is the electronic coupling between the initial and final states, 52

$$V \propto \left(\psi_i \left| \frac{e^2}{\mathbf{r}_{D-A}} \right| \psi_f \right) = \left(\psi_{D_T^*} \psi_A \left| \frac{e^2}{\mathbf{r}_{D-A}} \right| \psi_D \psi_{A_T^*} \right), \tag{4}$$

where $\psi_{D_T^*}$ (ψ_D) and $\psi_{A_T^*}$ (ψ_A) are the wavefunctions of the excited triplet state (the ground state) in the donor and acceptor, respectively. It is expected that the coupling term V decays exponentially along the donor–acceptor distance r_{D-A} . As a result, under the assumption of constant FCWD, the rate constant should show the similar distance dependence,

$$k_{TET}(r) \propto |V(r)|^2 = |V(0)|^2 e^{-\beta r}.$$
 (5)

In Eq. (5), V(r) and V(0) are the coupling terms at a donor-acceptor distance of r and 0, respectively, and β is the decay constant. Indeed, many recent studies on the distance-dependent triplet energy transfer in QD-acceptor systems confirmed the exponential decay of k_{TET} when tuning the distance with QD shell QD surface ligand length,⁵⁵ or intervening phenyl bridge length. ^{21,22,47} Figure 4(a) shows the exponential fit to the measured k_{TET} vs the QD-transmitter distance in CdSe-9ACA, CdSe-CAA, and CdSe-CDAA. The distance is defined from the carboxylic anchoring group to the anthracene core. The fitting shows a decay constant β_{kTET} of 0.118 \pm 0.011 Å⁻¹ (see details in Sec. 6 of the supplementary material), which is much smaller than those measured along phenyl bridges (0.32-0.72 Å⁻¹), ^{21,22,47} saturated hydrocarbon bridges (0.52 Å^{-1}) , 55 and inorganic shells $(0.62-3.4 \text{ Å}^{-1})$. 53,54 In terms of CdSe photonsensitizer and anthracene transmitter donor-acceptor systems, Li et al. demonstrated in 2016 that when the distance between CdSe QDs and the anthracene transmitter ligand is increased with rigid phenyl bridges, the TET₁ rate constant is distance dependent following the Dexter energy transfer model with the damping coefficient $\beta = 0.43 \pm 0.07 \text{ Å}^{-1}.^{21}$ We have also shown that the triplet energy transfer pathway changes from tunneling to hopping²² with a damping coefficient β of 0.7236 \pm 0.0005 Å⁻¹ when the driving force for TET is larger.

This shallow distance dependence of k_{TET} introduced by the acetylene spacers may originate from a different coupling

mechanism between the QD and the anthracene core. A recent study by He et al. suggests that the through-space coupling dominates when the QD exciton wavefunction leakage is large and directly overlaps with the anthracene core.⁴⁸ However, when the exciton wavefunction leakage is small, such as in type I core/shell structure, the through-bond coupling starts to contribute to the triplet energy transfer. Under this assumption, the 2.68 nm CdSe QD in this study should also present a large exciton wavefunction leakage and prefer a through-space coupling. According to Eq. (4), assuming that $\psi_{A_T^*}$ dominates on the anthracene core in 9ACA, CAA, and CDAA, the through-space coupling indicates that the distance dependence mainly originates from $\psi_{D_x^*}$, or the radial distribution function (RDF) of the exciton wavefunction, as illustrated in Fig. 4(b). To test this model, we examined the RDF of the exciton wavefunction in our QD. Details of the RDF calculation are given in Sec. 7 of the supplementary material. Figure 4(a) shows an exponential fit to the squared RDF (RDF²). The decay constant β_{RDF^2} is 5.00 \pm 0.32 Å $^{-1}$, much larger than $\beta_{k,TET}$, indicating that the slow decay of k_{TET} in CdSe-CAA and CdSe-CDAA cannot be explained by the through-space coupling mechanism. We also note that although previous studies with different types of spacers between QD and triplet acceptors show much larger $\beta_{k,TET}$ than the acetylene spacers here, those measured $\beta_{k,TET}$ s (0.32–0.72 Å $^{-1}$) are also significantly smaller than the β_{RDF^2} calculated above. This comparison may also exclude the through-space coupling mechanism in those systems.

On the other hand, we also examined the through-bond coupling mechanism. The through-bound coupling mediated triplet energy transfer is well understood in molecular donor-bridge-acceptor systems, 56-58 where the donor's orbital is mixed with the bridge's orbital.⁵⁹ To compare different transmitters on QD surfaces in this model, we focused on the transmitter wavefunction $\psi_{A_x^*}$ near the QD surface. In particular, the T₁ state spin density (ρ) integrated around the carbon atom (within the integration spheric radius of 1.8 Å, yellow dashed circle in Fig. 4(b) in the carboxylic anchoring group) is compared between 9ACA, CAA, and CDAA. The calculation of ρ is given in Sec. 8 of the supplementary material. Figure 4(a) shows the exponential fit to the squared ρ (ρ^2) with a decay constant β_{ρ^2} of 0.161 \pm 0.035 Å⁻¹, closely matching the measured $\beta_{k,TET}$ of 0.118 \pm 0.011 Å⁻¹. This result indicates a through-bond coupling mechanism between the CdSe QD and the anthracene core with acetylene spacers, which may be promoted by the conjugation among the COO^{Θ} group, the acetylene group, and the anthracene core. Indeed, Fig. 4(b) shows that the T1 state spin density in CAA and CDAA extends from the anthracene core to the COO[⊕] group through the acetylene spacer. In contrast, the conjugation with phenyl spacers is hindered by sterics,²² which may reduce the $\psi_{A_x^*}$ amplitude at the anchoring group and weaken the coupling.

Based on the through-bond coupling mechanism, we now involve the FCWD factor to further explain the shallow distance dependence of k_{TET} . The FCWD factor can be written following a Marcus-like theory,⁶⁰ and Eq. (3) is reformed as follows:

$$k = \frac{2\pi}{\hbar} |V|^2 FCWD = \frac{2\pi}{\hbar} |V|^2 \frac{1}{\sqrt{4\pi\lambda k_b T}} \exp\left[-\frac{(\lambda + \Delta G)^2}{4\lambda k_b T}\right].$$
 (6)

In Eq. (6), λ and ΔG are the reorganization energy and driving force for the triplet energy transfer reaction, respectively, and k_b is the Boltzmann constant. The coupling V is represented by the spin density ρ . λ and the T_1 energies are obtained from DFT calculations (Sec. 9 of the supplementary material). ΔG is calculated as the difference between the T_1 energies and QD exciton energies: $\Delta G = T_1 - E$. As discussed above, both band edge excitons and trapped excitons can transfer energy to the acceptors, and the rate constant obtained from the stretched exponential fitting is averaged over these different pathways. Therefore, the rate constant can be reproduced as follows:

$$k_{cal.} = \int P_{BE}(E)k_{BE}(\Delta G)dE + \int P_{TE}(E)k_{TE}(\Delta G)dE.$$
 (7)

 $P_{BE(TE)}(E)$ describes the probability distribution of the QD band edge (trapped) exciton state with energy E and can be estimated from the QD PL spectral profile, which includes both band edge (BE) exciton and trapped exciton (TE) emission, as shown in Fig. 1(b) and Fig. S18. More details are given in Sec. 10 of the supplementary material. $k(\Delta G)$ is given by Eq. (6). Figure 4(c) shows the calculated probability-weighted rate constant $P(E)k(\Delta G)$ as a function of ΔG for both the band edge excitons (solid lines) and trapped excitons (dashed lines). The reorganization energies are also indicated at the top x-axis in Fig. 4(c). The inset in Fig. 4(c) illustrates the energy alignment of QD excitons and transmitter triplets. In CdSe-9ACA, the high 9ACA T₁ energy (1.83 eV) renders a smaller absolute free energy change or driving force ($|\Delta G| = |E - T_1|$, where *E* is the band edge or trapped exciton energy), and the triplet energy transfer from both band edge exciton and trapped exciton falls into the Marcus normal region. As a result, the band edge exciton with a larger driving force contributes mostly to the overall rate constant. This is consistent with our previous PL lifetime measurements in CdSe QD-9ACA, 40 where the triplet energy transfer rate from band edge exciton is much larger than that from the trapped exciton. In CdSe-CAA and CdSe-CDAA, the transmitter T₁ energies are lower, 1.63 and 1.56 eV, respectively, resulting in large driving forces for TET. Consequently, the triplet energy transfer from band edge exciton falls into the Marcus-inverted region, while the transfer from trapped excitons remains in the normal region. Compared to CdSe-9ACA, the trapped excitons in CdSe-CAA and CdSe-CDAA show a larger driving force for TET in the normal region and, thus, show larger transfer rates, compensating for the quick decay of the band edge exciton transfer rate from CdSe-9ACA to CdSe-CAA and CdSe-CDAA.

The calculated average rate constants $k_{cal\cdot}$ are plotted against the acetylene bridge length in Fig. 4(a). An exponential fit to $k_{cal\cdot}$ gives a rate decay constant $\beta_{k,cal\cdot}$ of 0.103 \pm 0.026 Å⁻¹, agreeing well with $\beta_{k,TET}$ and β_{ρ^2} . The smaller $\beta_{k,cal\cdot}$ than β_{ρ^2} indicates that the FCWD factor alleviates the exponential decay of k_{TET} and that the exponential decay trend is dominated by the electronic coupling term. In the above simulation, the coupling V is set the same in both $k_{BE}(\Delta G)$ and $k_{TE}(\Delta G)$. Since the trapped exciton wavefunction should be more localized due to the trapped hole, V is expected to be smaller for $k_{TE}(\Delta G)$. A decreased V in $k_{TE}(\Delta G)$ will reduce the trapped exciton contribution and lead to a larger $\beta_{k,cal\cdot}$, closer to the experimental value. However, complete removal of the trapped exciton contribution leads to a $\beta_{k,cal\cdot}$ of 0.459 \pm 0.074 Å⁻¹, which is inconsistent with the experimental results and suggests

that the trapped exciton contribution is necessary. Note that only trapped excitons with energies larger than T₁ energies are considered in the modeling. We note that in the literature^{30,40} and the results here, the trapped exciton emission with energies lower than T_1 is also quenched by triplet acceptors, indicating an endothermic triplet energy transfer,⁵⁴ which is not involved in the above model. This model is further verified by simulating the XB decay kinetics (Sec. 11 of the supplementary material) using the exciton energy distribution and the triplet energy transfer rate constant calculated from the Marcus-like theory [Eq. (6)]. Figure S19 shows that the simulated kinetics qualitatively agree with the experimental results: slowest decay in CdSe-9ACA and fastest decay in CdSe-CAA. This consistency validates the triplet energy transfer model featuring a Marcus-like theory and the trapped exciton contribution.

Finally, we consider the possibility of cumulenic character in CAA and CDAA enhancing the triplet energy transfer rate from CdSe to the anthracene core. As shown in Table S6, there is a reduction of the bond length alternation (BLA) in the T1 state of CAA and CDAA, indicating increased cumulenic character. This may contribute to enhance the electronic coupling between the CdSe and anthracene units and, thus, promote more efficient TET. The cumulenic character increases from CAA to CDAA due to its larger polyyne length, in agreement with the literature and the BLA values reported for similar compounds with sp²-based end groups.¹¹

CONCLUSION

Our femtosecond transient absorption results demonstrate that the oligoyne bridges between CdSe QDs and anthracene cores introduce a damping coefficient β of 0.118 \pm 0.011 Å⁻¹ for the triplet energy transfer rate constant. We attribute this shallow distance dependence to the strong through-bond coupling between CdSe QDs and CAA or CDAA promoted by the acetylene spacer. The oligoyne spacers can extend the anthracene core wavefunction to the COO[⊕] anchoring group to enhance the coupling strength. In addition, we found out that oligovne spacers lower the T_1 energy level, which opens a possible triplet energy transfer pathway from the trap states. The trapped excitons contribute significantly to triplet energy transfer from CdSe to the CAA and CDAA transmitter ligands. Our DFT calculations support a slight cumulene character in the triplet excited states for CAA and CDAA, where the rate of triplet energy transfer is maintained even though the bond length is increased. Altogether, this work shows that oligoyne spacers allow energy transfer over longer distances while maintaining a fast energy transfer rate, especially when compared to conventional phenylene molecular bridges.

SUPPLEMENTARY MATERIAL

The supplementary material encompasses experimental methods, synthesis, data fitting procedures, and computational details.

ACKNOWLEDGMENTS

M. L. T. acknowledges the support from the National Science Foundation, Grant No. CHE-2147792, as well as prior support

from Air Force Office of Scientific Research Award No. FA9550-20-1-0112. T. L. acknowledges the support from the National Science Foundation (Grant Nos. CHE-2305112, CHE-2004080, and CHE-1726536). M. F. acknowledges the financial support from the Ministerio de Ciencia e Innovación and Agencia Estatal de Investigación (MCIN/AEI/10.13039/501100011033) for RYC2021-030924-I and PID2022-140460NA-I00 projects and the Unidad de Excelencia María de Maeztu, Grant No. CEX2021-001202-M, granted to the ITQCUB, as well as the Generalitat de Catalunya for Grant No. 2021SGR00354 and the University of Barcelona/IQTCUB for the computational resources. A. L. K. acknowledges the use of computational resources at the Cherry L. Emerson Center.

AUTHOR DECLARATIONS

Conflict of Interest

The authors have no conflicts to disclose.

Author Contributions

T.M. and S.H. contributed equally to the work.

Tsumugi Miyashita: Conceptualization (equal); Data curation (equal); Formal analysis (equal); Writing - original draft (equal); Writing - review & editing (equal). Sheng He: Conceptualization (equal); Data curation (equal); Formal analysis (equal); Writing original draft (equal); Writing - review & editing (equal). Paulina Jaimes: Conceptualization (equal); Data curation (equal); Formal analysis (equal); Writing - original draft (equal); Writing - review & editing (equal). Alexey L. Kaledin: Formal analysis (equal); Writing - original draft (equal); Writing - review & editing (equal). Maria Fumanal: Formal analysis (equal); Funding acquisition (equal); Writing - original draft (equal); Writing - review & editing (equal). Tianquan Lian: Funding acquisition (equal); Project administration (equal); Supervision (equal); Writing – original draft (equal); Writing - review & editing (equal). Ming Lee Tang: Funding acquisition (equal); Project administration (equal); Supervision (equal); Writing - original draft (equal); Writing - review & editing (equal).

DATA AVAILABILITY

The data that support the findings of this study are available within the article and its supplementary material.

REFERENCES

¹P. Moreno-García, M. Gulcur, D. Z. Manrique, T. Pope, W. Hong, V. Kaliginedi, C. Huang, A. S. Batsanov, M. R. Bryce, C. Lambert, and T. Wandlowski, "Single-molecule conductance of functionalized oligoynes: Length dependence and junction evolution," J. Am. Chem. Soc. 135(33), 12228-12240 (2013).

² J. A. Malen, P. Doak, K. Baheti, T. D. Tilley, R. A. Segalman, and A. Majumdar, "Identifying the length dependence of orbital alignment and contact coupling in molecular heterojunctions," Nano Lett. 9(3), 1164-1169 (2009).

³H. J. Lee, S. J. Cho, H. Kang, X. He, and H. J. Yoon, "Achieving ultralow, zero, and inverted tunneling attenuation coefficients in molecular wires with extended conjugation," Small 17(12), 2005711 (2021).

- ⁴J. R. Widawsky, W. Chen, H. Vázquez, T. Kim, R. Breslow, M. S. Hybertsen, and L. Venkataraman, "Length-dependent thermopower of highly conducting Au–C bonded single molecule junctions," Nano Lett. 13(6), 2889–2894 (2013).
- ⁵Y. Zang, T. Fu, Q. Zou, F. Ng, H. Li, M. L. Steigerwald, C. Nuckolls, and L. Venkataraman, "Cumulene wires display increasing conductance with increasing length," Nano Lett. **20**(11), 8415–8419 (2020).
- ⁶W. Xu, E. Leary, S. Hou, S. Sangtarash, M. T. González, G. Rubio-Bollinger, Q. Wu, H. Sadeghi, L. Tejerina, K. E. Christensen *et al.*, "Unusual length dependence of the conductance in cumulene molecular wires," Angew. Chem., Int. Ed. **58**(25), 8378–8382 (2019).
- ⁷J. Prasongkit, A. Grigoriev, G. Wendin, and R. Ahuja, "Cumulene molecular wire conductance from first principles," Phys. Rev. B **81**(11), 115404 (2010).
- ⁸M. H. Garner, W. Bro-Jørgensen, P. D. Pedersen, and G. C. Solomon, "Reverse bond-length alternation in cumulenes: Candidates for increasing electronic transmission with length," J. Phys. Chem. C 122(47), 26777–26789 (2018).
- ⁹Y. Tsuji, R. Movassagh, S. Datta, and R. Hoffmann, "Exponential attenuation of through-bond transmission in a polyene: Theory and potential realizations," ACS Nano **9**(11), 11109–11120 (2015).
- ¹⁰ A. Zieleniewska, X. Zhao, S. Bauroth, C. Wang, A. S. Batsanov, C. Krick Calderon, A. Kahnt, T. Clark, M. R. Bryce, and D. M. Guldi, "Resonance-enhanced charge delocalization in carbazole-oligoyne-oxadiazole conjugates," J. Am. Chem. Soc. 142(44), 18769–18781 (2020).
- A. Milani, M. Tommasini, V. Barbieri, A. Lucotti, V. Russo, F. Cataldo, and C. S. Casari, "Semiconductor-to-metal transition in carbon-atom wires driven by sp² conjugated end groups," J. Phys. Chem. C 121(19), 10562–10570 (2017).
 N. R. Champness, A. N. Khlobystov, A. G. Majuga, M. Schröder, and N. V.
- N. R. Champness, A. N. Khlobystov, A. G. Majuga, M. Schröder, and N. V. Zyk, "An improved preparation of 4-ethynylpyridine and its application to the synthesis of linear bipyridyl ligands," Tetrahedron Lett. 40(29), 5413–5416 (1999).
 C. Wang, A. S. Batsanov, M. R. Bryce, S. Martín, R. J. Nichols, S. J. Higgins, V. M. García-Suárez, and C. J. Lambert, "Oligoyne single molecule wires," J. Am. Chem. Soc. 131(43), 15647–15654 (2009).
- ¹⁴ M. Krempe, R. Lippert, F. Hampel, I. Ivanović-Burmazović, N. Jux, and R. R. Tykwinski, "Pyridyl-endcapped polyynes: Stabilized wire-like molecules," Angew. Chem., Int. Ed. 55(47), 14802–14806 (2016).
- ¹⁵Y. Gao and R. R. Tykwinski, "Advances in polyynes to model carbyne," Acc. Chem. Res. 55(24), 3616–3630 (2022).
- ¹⁶Y. Gao, Y. Hou, F. Gordillo Gámez, M. J. Ferguson, J. Casado, and R. R. Tykwinski, "The loss of endgroup effects in long pyridyl-endcapped oligoynes on the way to carbyne," Nat. Chem. 12(12), 1143–1149 (2020).
- ¹⁷J. S. Dhindsa, E. L. Cotterill, F. L. Buguis, M. Anghel, P. D. Boyle, and J. B. Gilroy, "Blending the optical and redox properties of oligoynes and boron difluoride formazanates," Angew. Chem., Int. Ed. 61(39), e202208502 (2022).
- ¹⁸M. Biswas, P. Nguyen, T. B. Marder, and L. R. Khundkar, "Unusual size dependence of nonradiative charge recombination rates in acetylene-bridged compounds," J. Phys. Chem. A 101(9), 1689–1695 (1997).
- ¹⁹ M. Štefko, M. D. Tzirakis, B. Breiten, M.-O. Ebert, O. Dumele, W. B. Schweizer, J.-P. Gisselbrecht, C. Boudon, M. T. Beels, I. Biaggio, and F. Diederich, "Donor–acceptor (D–A)-substituted polyyne chromophores: Modulation of their optoelectronic properties by varying the length of the acetylene spacer," Chem. Eur. J. 19(38), 12693–12704 (2013).
- ²⁰S. A. Vail, P. J. Krawczuk, D. M. Guldi, A. Palkar, L. Echegoyen, J. P. C. Tomé, M. A. Fazio, and D. I. Schuster, "Energy and electron transfer in polyacetylenelinked zinc-porphyrin-[60] fullerene molecular wires," Chem. Eur. J. 11(11), 3375–3388 (2005).
- ²¹ X. Li, Z. Huang, R. Zavala, and M. L. Tang, "Distance-dependent triplet energy transfer between CdSe nanocrystals and surface bound anthracene," J. Phys. Chem. Lett. 7(11), 1955–1959 (2016).
- Z. Huang, Z. Xu, T. Huang, V. Gray, K. Moth-Poulsen, T. Lian, and M. L. Tang, "Evolution from tunneling to hopping mediated triplet energy transfer from quantum dots to molecules," J. Am. Chem. Soc. 142(41), 17581–17588 (2020).
 Z. Tasaki, K. Nishimura, H. Toyoshima, T. Masuda, M. Nakamura, Y. Nakano,
- ²⁵ S. Tasaki, K. Nishimura, H. Toyoshima, T. Masuda, M. Nakamura, Y. Nakano, H. Itoi, E. Kambe, Y. Kawamura, and H. Kuma, "Realization of ultra-high-efficient fluorescent blue OLED," J. Soc. Inf. Disp. 30(5), 441–451 (2022).
- ²⁴N. A. Kukhta, T. Matulaitis, D. Volyniuk, K. Ivaniuk, P. Turyk, P. Stakhira, J. V. Grazulevicius, and A. P. Monkman, "Deep-blue high-efficiency TTA OLED using

- *para-* and *meta-*conjugated cyanotriphenylbenzene and carbazole derivatives as emitter and host," J. Phys. Chem. Lett. **8**(24), 6199–6205 (2017).
- L. Huang, W. Wu, Y. Li, K. Huang, L. Zeng, W. Lin, and G. Han, "Highly effective near-infrared activating triplet-triplet annihilation upconversion for photoredox catalysis," J. Am. Chem. Soc. 142(43), 18460–18470 (2020).
 A. J. Carrod, V. Gray, and K. Börjesson, "Recent advances in triplet-triplet
- ²⁶ A. J. Carrod, V. Gray, and K. Börjesson, "Recent advances in triplet-triplet annihilation upconversion and singlet fission, towards solar energy applications," Energy Environ. Sci. 15 (12), 4982–5016 (2022).
- ²⁷D. Beery, T. W. Schmidt, and K. Hanson, "Harnessing sunlight via molecular photon upconversion," ACS Appl. Mater. Interfaces 13(28), 32601–32605 (2021).

 ²⁸I. Huang, T. Le, K. Huang, and G. Han, "Enzymatic enhancing of triplet, triplet.
- ²⁸L. Huang, T. Le, K. Huang, and G. Han, "Enzymatic enhancing of triplet-triplet annihilation upconversion by breaking oxygen quenching for background-free biological sensing," Nat. Commun. **12**(1), 1898 (2021).
- ²⁹L. Zeng, L. Huang, J. Han, and G. Han, "Enhancing triplet–triplet annihilation upconversion: From molecular design to present applications," Acc. Chem. Res. 55(18), 2604–2615 (2022).
- ³⁰C. Mongin, S. Garakyaraghi, N. Razgoniaeva, M. Zamkov, and F. N. Castellano, "Direct observation of triplet energy transfer from semiconductor nanocrystals," Science 351(6271), 369–372 (2016).
- ³¹ Z. Y. Huang, X. Li, M. Mahboub, K. M. Hanson, V. M. Nichols, H. Le, M. L. Tang, and C. J. Bardeen, "Hybrid molecule-nanocrystal photon upconversion across the visible and near-infrared," Nano Lett. **15**(8), 5552–5557 (2015).
- ³² M. F. Wu, D. N. Congreve, M. W. B. Wilson, J. Jean, N. Geva, M. Welborn, T. Van Voorhis, V. Bulovic, M. G. Bawendi, and M. A. Baldo, "Solid-state infrared-to-visible upconversion sensitized by colloidal nanocrystals," Nat. Photonics 10(1), 31–34 (2016).
- ⁵³T. Jin, S. He, Y. Zhu, E. Egap, and T. Lian, "Bright state sensitized triplet energy transfer from quantum dot to molecular acceptor revealed by temperature dependent energy transfer dynamics," Nano Lett. 22(10), 3897–3903 (2022).
- ³⁴W. Rodríguez-Córdoba, R. Noria-Moreno, P. Navarro, and J. Peon, "Ultrafast fluorescence study of the effect of carboxylic and carboxylate substituents on the excited state properties of anthracene," J. Lumin. 145, 697–707 (2014).
- ³⁵V. I. Klimov, "Spectral and dynamical properties of multiexcitons in semiconductor nanocrystals," Annu. Rev. Phys. Chem. 58, 635–673 (2007).
- ³⁶M. Montalti and S. L. Murov, Handbook of Photochemistry (CRC/Taylor & Francis, 2006).
- ³⁷K. J. Fallon, E. M. Churchill, S. N. Sanders, J. Shee, J. L. Weber, R. Meir, S. Jockusch, D. R. Reichman, M. Y. Sfeir, D. N. Congreve, and L. M. Campos, "Molecular engineering of chromophores to enable triplet–triplet annihilation upconversion," J. Am. Chem. Soc. 142(47), 19917–19925 (2020).
- ³⁸T. Miyashita, P. Jaimes, T. Lian, M. L. Tang, and Z. Xu, "Quantifying the ligand-induced triplet energy transfer barrier in a quantum dot-based upconversion system," J. Phys. Chem. Lett. **13**(13), 3002–3007 (2022).
- ³⁹ H. Zhu, N. Song, and T. Lian, "Controlling charge separation and recombination rates in CdSe/ZnS type I core—shell quantum dots by shell thicknesses," J. Am. Chem. Soc. **132**(42), 15038–15045 (2010).
- 40 T. Jin and T. Lian, "Trap state mediated triplet energy transfer from CdSe quantum dots to molecular acceptors," J. Chem. Phys. 153(7), 074703 (2020).
 41 C. Wang, L. O. Pålsson, A. S. Batsanov, and M. R. Bryce, "Molecular wires
- ⁴¹C. Wang, L. O. Pålsson, A. S. Batsanov, and M. R. Bryce, "Molecular wires comprising π -extended ethynyl- and butadiynyl-2,5-diphenyl-1,3,4-oxadiazole derivatives: Synthesis, redox, structural, and optoelectronic properties," J. Am. Chem. Soc. **128**(11), 3789–3799 (2006).
- 42 L. O. Pålsson, C. Wang, A. S. Batsanov, S. M. King, A. Beeby, A. P. Monkman, and M. R. Bryce, "Efficient intramolecular charge transfer in oligoyne-linked donor–π–acceptor molecules," Chem. Eur. J. 16(5), 1470–1479 (2010).
- ⁴³ A. E. Stiegman, V. M. Miskowski, J. W. Perry, and D. R. Coulter, "A series of donor-acceptor molecules of the form NH2(C6H4)(C.tplbond.C)n(C6H4)NO2. Unusual effects of varying n," J. Am. Chem. Soc. **109**(19), 5884–5886 (1987).
- ⁴⁴V. I. Klimov, A. A. Mikhailovsky, D. W. McBranch, C. A. Leatherdale, and M. G. Bawendi, "Quantization of multiparticle auger rates in semiconductor quantum dots," Science 287(5455), 1011–1013 (2000).
- ⁴⁵X. Li, V. M. Nichols, D. Zhou, C. Lim, G. S. Pau, C. J. Bardeen, and M. L. Tang, "Observation of multiple, identical binding sites in the exchange of carboxylic acid ligands with CdS nanocrystals," Nano Lett. 14(6), 3382–3387 (2014).

- ⁴⁶G. B. Piland, Z. Y. Huang, M. Lee Tang, and C. J. Bardeen, "Dynamics of energy transfer from CdSe nanocrystals to triplet states of anthracene ligand molecules," J. Phys. Chem. C 120(11), 5883–5889 (2016).
- ⁴⁷Z. Xu, Z. Huang, C. Li, T. Huang, F. A. Evangelista, M. L. Tang, and T. Lian, "Tuning the quantum dot (QD)/mediator interface for optimal efficiency of QD-sensitized near-infrared-to-visible photon upconversion systems," ACS Appl. Mater. Interfaces 12(32), 36558–36567 (2020).
- ⁴⁸S. He, R. Lai, Q. Jiang, Y. Han, X. Luo, Y. Tian, X. Liu, and K. Wu, "Engineering sensitized photon upconversion efficiency via nanocrystal wavefunction and molecular geometry," Angew. Chem., Int. Ed. **59**(40), 17726–17731 (2020).
- ⁴⁹P. Xia, Z. Huang, X. Li, J. J. Romero, V. I. Vullev, G. S. Pau, and M. L. Tang, "On the efficacy of anthracene isomers for triplet transmission from CdSe nanocrystals," Chem. Commun. 53(7), 1241–1244 (2017).
- ⁵⁰D. L. Dexter, "A theory of sensitized luminescence in solids," J. Chem. Phys. 21(5), 836–850 (1953).
- ⁵¹ R. D. Harcourt, G. D. Scholes, and K. P. Ghiggino, "Rate expressions for excitation transfer. II. Electronic considerations of direct and through–configuration exciton resonance interactions," J. Chem. Phys. 101(12), 10521–10525 (1994).
- ⁵²Z. Q. You and C. P. Hsu, "Theory and calculation for the electronic coupling in excitation energy transfer," Int. J. Quantum Chem. 114(2), 102–115 (2014).
- ⁵³M. Mahboub, Z. Huang, and M. L. Tang, "Efficient infrared-to-visible upconversion with subsolar irradiance," Nano Lett. 16(11), 7169–7175 (2016).

- ⁵⁴R. Lai, Y. Liu, X. Luo, L. Chen, Y. Han, M. Lv, G. Liang, J. Chen, C. Zhang, D. Di *et al.*, "Shallow distance-dependent triplet energy migration mediated by endothermic charge-transfer," Nat. Commun. 12(1), 1532 (2021).
- ⁵⁵L. Nienhaus, M. Wu, N. Geva, J. J. Shepherd, M. W. B. Wilson, V. Bulovic, T. Van Voorhis, M. A. Baldo, and M. G. Bawendi, "Speed limit for triplet-exciton transfer in solid-state PbS nanocrystal-sensitized photon upconversion," ACS Nano 11(8), 7848–7857 (2017).
- ⁵⁶G. L. Closs, P. Piotrowiak, J. M. MacInnis, and G. R. Fleming, "Determination of long-distance intramolecular triplet energy-transfer rates. Quantitative comparison with electron transfer," J. Am. Chem. Soc. 110(8), 2652–2653 (1988).
- ⁵⁷G. L. Closs, M. D. Johnson, J. R. Miller, and P. Piotrowiak, "A connection between intramolecular long-range electron, hole, and triplet energy transfers," J. Am. Chem. Soc. 111(10), 3751–3753 (1989).
- ⁵⁸G. D. Scholes, K. P. Ghiggino, A. M. Oliver, and M. N. Paddon-Row, "Through-space and through-bond effects on exciton interactions in rigidly linked dinaphthyl molecules," J. Am. Chem. Soc. 115(10), 4345–4349 (1993).
- ⁵⁹H. M. McConnell, "Intramolecular charge transfer in aromatic free radicals," J. Chem. Phys. 35(2), 508–515 (1961).
- ⁶⁰ Z. Xu, Z. Huang, T. Jin, T. Lian, and M. L. Tang, "Mechanistic understanding and rational design of quantum dot/mediator interfaces for efficient photon upconversion," Acc. Chem. Res. **54**, 70 (2021).